Proceedings of the 2018 IEEE
International Conference on Robotics and Biomimetics
December 12-15, 2018, Kuala Lumpur, Malaysia

Design of a Sliding-Pin Needle Driver for a Continuum Surgical Robot*

Zhaoyu Zhang, Zhonghao Wu, Lingyun Zeng, Weihao Zhang and Kai Xu*, *Member, IEEE,*

***Abstract*—MIS (Minimally Invasive Surgery) is advantageous in terms of improved treatment outcomes and reduced recovery time. Many surgical robotic systems have hence been developed to assist MIS due to the operation difficulties while using manual laparoscopic tools. In recent years, continuum surgical robots have been found appealing due to their inherent compliance, light weight, design compactness, and distal dexterity. However, the gripper, needle driver and other similar surgical end effectors for a continuum surgical robot cannot be actuated with adequate actuation forces: pulling the actuation line too hard will increase the risk of structural buckling and failure. Since these surgical end effectors have to generate sufficient gripping forces to make them clinically useful, this paper presents the design of a sliding-pin needle driver, specifically for the integration into a continuum surgical robot. The design aims at a proper gripping capability under a limited actuation force. Model-based design determination and finite element analysis were conducted to finalize the design features. A comparison of the output gripping forces among the sliding-pin needle driver, the *large needle driver* of the da Vinci EndoWrist tool and a manual laparoscopic needle driver, together with the experimental validations, indicates the effectiveness of the proposed design. It is expected that similar surgical end effectors for continuum surgical robots can be designed following the presented design approach.**

I. Introduction

MIS (Minimally Invasive Surgery) offers significant advantages over open surgery such as the improved cosmesis, quicker recovery, and less postoperative complications [1]. Due to the operation difficulties while using manual laparoscopic tools (e.g., inverted tool movements, hindered haptic perception), many surgical robotic systems have hence been developed to assist MIS for enhanced motion precision, augmented sensing and improved distal dexterity [2, 3].

Gripper-like surgical end effectors (e.g., needle driver and tissue grasper), either in manual laparoscopic tools or in surgical robotic systems, play essential roles in completing the surgical tasks. In the manual laparoscopic needle driver in Fig. 1(a), a relatively thick stainless steel rod (usually 2 mm or more in diameter) was pulled by the handle to actuate the opening jaw for enough gripping forces. On the other hand, in many existing laparoscopic surgical robotic systems where a manipulator maneuvers a stick-like surgical tool for intra-abdominal surgical tasks [4-7], the surgical end effector is often actuated by pulling a pair of actuation cables. Since the stick-like surgical tool usually has a rigid structure, e.g., the EndoWrist instrument of the da Vinci system in Fig 1(b), it is always possible to increase the actuation cable tension for enhanced gripping capability [8, 9].

In recent years, continuum robots have been found appealing for surgical applications, due to their inherent compliance, light weight, design compactness, and distal dexterity [10-14]. In a surgical continuum manipulator, a distal end effector is usually installed on top of two or more bending segments that are used for dexterous movements. The distal surgical end effector, e.g., a gripper or a needle driver, cannot be actuated with adequate actuation force, since pulling the actuation line too hard will increase the risk of structural buckling and failure. As these surgical end effectors have to generate sufficient gripping forces to make them clinically useful, this paper presents the design of a sliding-pin needle driver, specifically for the integration into a continuum surgical robot, as shown in Fig. 1(c).

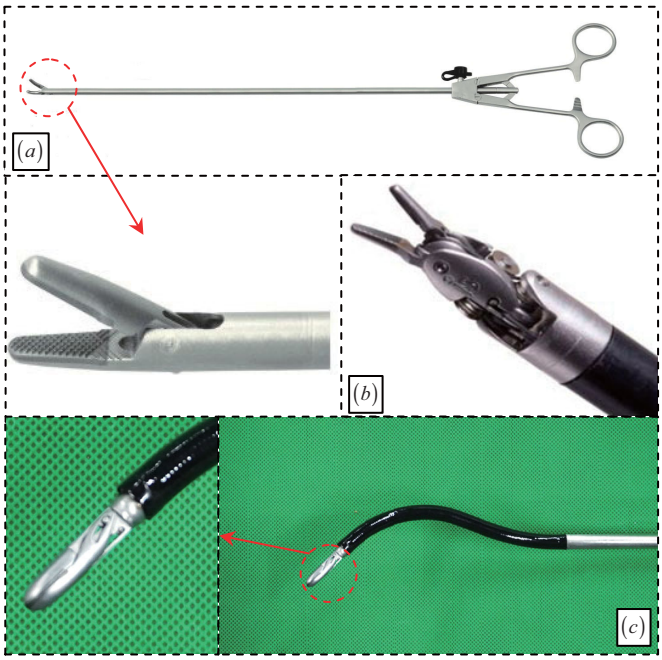

Figure 1. Needle drivers: (a) manual laparoscopic needle driver, (b) the da Vinci *large needle driver*, (c) the proposed sliding-pin needle driver

*This work was supported in part by the National Natural Science Foundation of China (Grant No. 51722507, Grant No. 51435010 and Grant No. 91648103), and in part by the National Key R&D Program of China (Grant No. 2017YFC0110800).

Zhaoyu Zhang and Zhonghao Wu are with the RII Lab (Lab of Robotics Innovation and Intervention), UM-SJTU Joint Institute, Shanghai Jiao Tong University, Shanghai, China (emails: zhangzhaoyu@sjtu.edu.cn and zhonghao.wu@sjtu.edu.cn).

Lingyun Zeng, Weihao Zhang and Kai Xu are with School of Mechanical Engineering, Shanghai Jiao Tong University, Shanghai, China (emails: me_maxqi@sjtu.edu.cn, zwh0813@sjtu.edu.cn and k.xu@sjtu.edu.cn, corresponding author: K. Xu).

978-1-7281-0377-8/18/$31.00 ©

The proposed design aims at generating a proper gripping capability under a limited actuation force. Model-based design determination and finite element analysis were conducted to finalize the design features. A comparison of the output gripping forces among the sliding-pin needle driver, the *large needle driver* of the da Vinci EndoWrist tool and a manual laparoscopic needle driver, together with the experimental validations, indicates the effectiveness of the proposed design.

This paper is organized as follows. Section II summarizes the design goals, while Section III presents the design descriptions of the sliding-pin needle driver of a continuum surgical robotic system. The comparison among the proposed design, a da Vinci EndoWrist tool and a laparoscopic needle driver is also reported. Section IV presents the characterizations including a finite element analysis of the needle driver structure and a series of experimental validations. Conclusions and future works are summarized in Section V.

II. Design Objectives

The sliding-pin needle driver is located at the distal end of a surgical continuum manipulator. The outer diameter of the continuum manipulator is 7.8 mm for its passage through a standard 8-mm-diameter trocar. The outer diameter of the needle driver is then set at 6mm to spare space for arranging a connection structure to the continuum manipulator and an insulation layer such that the design can be modified to become an electrical surgical end effector.

The opening angle of the sliding-pin needle driver is set to be up to 30°, referring to a manual laparoscopic needle driver design. In this way, the proposed needle driver can easily grip a suture needle, e.g., a 3/8 circular one or a half circle one. Please note that the da Vinci *large needle driver* can open its jaws more than 180° due to its mechanical design and actuation scheme. But the da Vinci *large needle driver* is never controlled to do so in a procedure.

While suturing, the needle driver shall firmly grip and release the circular needle repeatedly. The output force should be large enough when the jaw opening angle is small. Because the actuation force is generated by pulling a nitinol rod, the design of the sliding-pin needle driver should be capable of amplifying the actuation force and providing a sufficient gripping force. Even though the tissue perforation force during suturing is not large, the needle driver needs to provide a gripping force of 40 N [15]. This value is hence used here as the design objective for the gripping force.

III. Design Description

The sliding-pin needle drivers, as shown in Fig. 2, consist of i) a fixed jaw, ii) an opening jaw, iii) a sliding block, iv) a joint pin, and v) two sliding pins (the sliding pins #1 and #2).

The opening jaw has a slot (a.k.a. Slot-1) with a designed curve, while the fixed jaw has two vertical slots (Slot-2 and Slot-3). The sliding pin #1 and the sliding pin #2 are inserted into the sliding block. The sliding block is connected with a nitinol rod for push-and-pill actuation: pushing for opening and pulling for closing. While the sliding pin #1 and the sliding pin #2 slides freely in the Slot-2 and Slot-3 respectively, the sliding pin #1 also slides in the Slot-1 in the opening jaw. The opening jaw rotates with respect to the joint pin, which realizes the jaw's opening and closing motions. In order not to block the view during suturing, the jaws of the needle driver usually have tapering tips. The needle driver also has rounded edges to avoid physical harm to the suture tissue.

The sliding-pin needle driver, with an outer diameter of 6 mm and a length of approximately 20 mm, is located at the distal end of a surgical continuum manipulator. Majority of the needle driver is fabricated from medical-grade stainless steel. The teeth pads of the jaws are made from tungsten carbide with standard teeth patterns.

The curved slot in the opening jaw plays an essential role in generating the amplified gripping force. Its modeling is presented in Section III.A. Section III.B reports the parameter determination of the curved slot, while a simplified curve for the slot is proposed in Section III.C to ease the fabrication. The optimal gripping location is obtained in Section III.D, and a comparison of the output gripping forces among the proposed sliding-pin needle driver, the *large needle driver* of the da Vinci EndoWrist tool and a manual laparoscopic needle driver is presented in Section III.E.

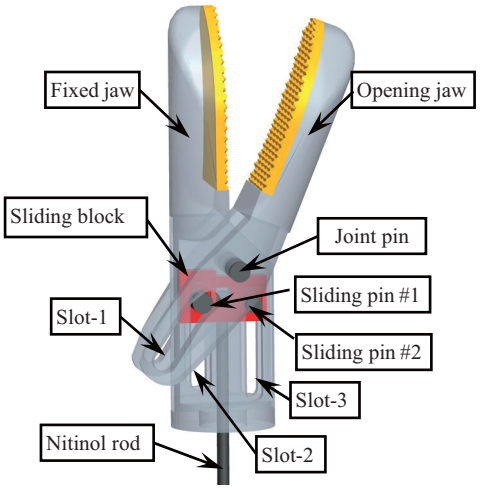

Figure 2. Design of the sliding-pin needle driver

A. Modeling of the Slot-1 Curve

As shown in Fig. 3, the following coordinates are defined to describe the model.

- *Base Coordinate* $\{B\} \equiv \{\hat{\mathbf{x}}_B, \hat{\mathbf{y}}_B\}$ is fixed with the fixed jaw of the needle driver. The coordinate origin is located at the joint pin of the fixed jaw.
- *Jaw Coordinate* $\{J\} \equiv \{\hat{\mathbf{x}}_J, \hat{\mathbf{y}}_J\}$ is assigned to the opening jaw of the needle driver. The coordinate origin is also located at the joint pin of the jaw.

The presented analysis is based on the virtual work principle. Neglecting the friction, the input power P_{in} of the opening jaw equals to its output power P_{out} as in (1).

$$P_{in} = P_{out} \tag{1}$$

The input power and the output power can also be written in (2) and (3), respectively.

$$P_{in} = f_{in} \cdot v_{in} = f_{in} \cdot \frac{d}{dt}\left({}^{B}y_{\mathbf{p}}\right) \tag{2}$$

Where f_{in} is the input force from the sliding block, v_{in} is the velocity of the sliding block, and ${}^{B}\mathbf{p}$ is the position of the sliding pin #1 in the Slot-2 with the coordinate of $[d\ {}^{B}y_{\mathbf{p}}]^{T}$.

$$P_{out} = \tau_{out} \cdot \omega_{out} = f_{out} \cdot l \cdot \frac{d\theta}{dt} \tag{3}$$

Where τ_{out} is the output torque of the opening jaw, f_{out} is the output gripping force that is perpendicular to the jaw surface, l is a distance between the needle gripping position and the joint pin, and θ is the opening angle of the opening jaw.

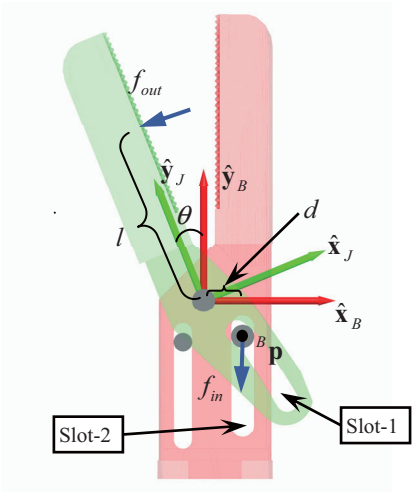

Figure 3. Coordinates assignment and force analysis of the jaws

Then the virtual work principle can be rewritten as in (4), substituting (2) and (3) into (1).

$$\Delta\, {}^{B}y_{\mathbf{p}} = \frac{f_{out} \cdot l \cdot \Delta\theta}{f_{in}} \tag{4}$$

When the opening jaw rotates, a ${}^{B}y_{\mathbf{p}}$ value always corresponds to a θ angle. Then ${}^{B}y_{\mathbf{p}}$ can be expressed in (5), while the θ angle decreases from the maximal value to 0° ($\Delta\theta$ is negative during this movement).

$${}^{B}y_{\mathbf{p}} = {}^{B}y_{\mathbf{p}0} + \sum \frac{f_{out} \cdot l \cdot \Delta\theta}{f_{in}} \tag{5}$$

Where ${}^{B}y_{\mathbf{p}0} < 0$ is the value of ${}^{B}y_{\mathbf{p}}$ when the θ angle is at the maximal value.

The ${}^{B}\mathbf{p}$ in the *Base Coordinate* $\{B\}$ can be transformed to the *Jaw Coordinate* $\{J\}$ as in (6).

$${}^{J}\mathbf{p} = {}^{J}\mathbf{R}_{B}\ {}^{B}\mathbf{p} \tag{6}$$

Where ${}^{J}\mathbf{R}_{B} = \begin{bmatrix} \cos\theta & -\sin\theta \\ \sin\theta & \cos\theta \end{bmatrix}$.

When the desirable output and input forces are determined and the θ angle is discretized in decrements of a small value $\Delta\theta$ from the maximum value to 0°, the position coordinates along the slot curve can be obtained in the *Jaw Coordinate* $\{J\}$, as in (7).

$$\begin{cases} {}^{J}x_{\mathbf{p}} = d\cos\theta - ({}^{B}y_{\mathbf{p}0} + \sum \frac{f_{out} \cdot l \cdot \Delta\theta}{f_{in}})\sin\theta \\ {}^{J}y_{\mathbf{p}} = d\sin\theta + ({}^{B}y_{\mathbf{p}0} + \sum \frac{f_{out} \cdot l \cdot \Delta\theta}{f_{in}})\cos\theta \end{cases} \tag{7}$$

Where $[{}^{J}x_{\mathbf{p}}\ {}^{J}y_{\mathbf{p}}]^{T}$ is the coordinate of ${}^{J}\mathbf{p}$ in $\{J\}$.

B. Parameter Determination of the Slot Curve

According to the design objectives described in Section II, the opening angle of the opening jaw is from 0° to 30°. When the gripper holds a thin needle, the opening angle would be relatively small. When the opening jaw opens large enough to release the needle, the jaw would be subject to a very small force. Then the force characteristics are set as follows, indicating the gripper should generate the goal of the 40-N gripping force under the 10-N actuation force from the nitinol rod.

- f_{out} = 40 N and f_{in} = 10 N, when $\theta \in [0°, 5°]$.
- f_{out} = 4 N and f_{in} = 10 N, when $\theta \in (5°, 30°]$.

The tentative gripping position is at the first tooth such that the l distance is at 8 mm. Considering the structural strength, fabrication and assembly feasibility, the d value of is set at 1.2 mm. And the value of the ${}^{B}y_{\mathbf{p}0}$ is set at -1 mm.

A program is written in MATLAB to enumerate the θ angle from 30° to 0°. The coordinates of ${}^{J}\mathbf{p}$ on the Slot-1 in the *Jaw Coordinate* $\{J\}$ are calculated with the θ angle discretized in decrements of 0.06° from 30° to 0°. The slot curve of the opening jaw is plotted in Fig. 4(a).

Clearly the Slot-1 curve consists of two parts. Part I corresponds to the θ angle values varying from 0° to 5°, where the steep slope helps generate a high gripping force. Part II corresponds to the θ angle values varying from 5° to 30°, where the relatively gentle slope helps the needle driver quickly open its jaw.

C. Simplification of the Slot Curve

The Slot-1 curve of the sliding-pin needle driver in Fig. 4(a) is clearly complex. It should be simplified for fabrication considerations.

As shown in Fig. 4(a), when the θ angle is between 0° and 5°, Part I of the slot curve is close to a 100° slope. Therefore, Part I of the curve is replaced by a line segment with a 100° slope. When the θ angle is between 5° and 30°, Part II of the slot curve is replaced by a line segment with a 120° slope. The two line segments are connected by an arc with a radius of 3 mm, as shown in Fig. 4(b).

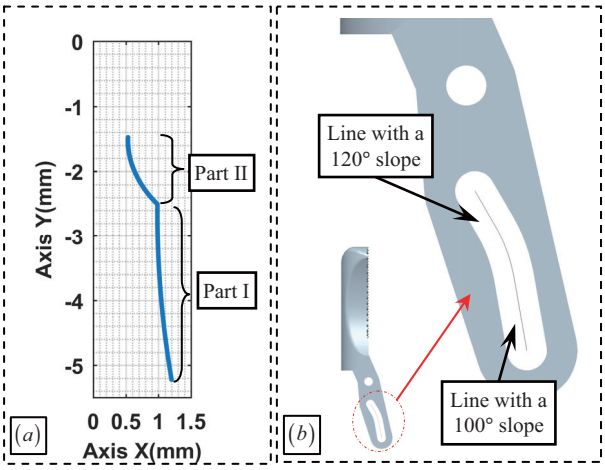

Figure 4. The Slot-1 curve of the opening jaw: (a) the designed curve, and (b) the simplified Slot-1 curve

Simulation was conducted in Pro/E and MATLAB to validate the simplification. The relationship between the gripping force and the θ angle is plotted in Fig. 5, under a constant actuation force of 10 N. The gripper force fulfills the design objective.

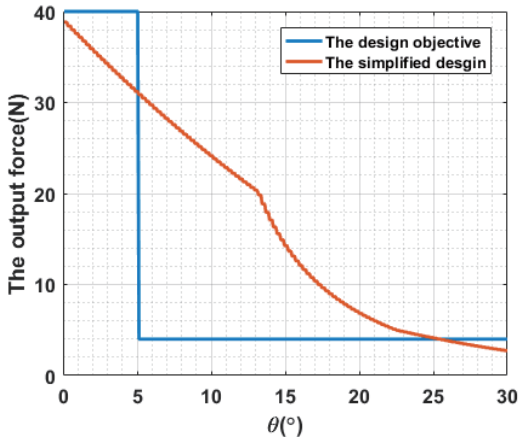

Figure 5. The relationship between the output gripping force and the θ angle of the simplified needle driver

D. Optimal Needle Gripping Position

In MIS, the 1/2 circle needle with #2-sized suture for laparoscopic surgeries with a radius of 0.6 mm is often used.

The gripping force is obtained from the equilibrium of the virtual work regarding the opening torque of the opening jaw. Then there is a paradox between the gripping force and the gripping position: if the needle is placed further away from the joint pin, the jaw opening angle will be smaller to produce a larger gripping force; but the moment arm (the l length) will be larger to produce a smaller gripping force. Hence, the optimal gripping position is investigated.

The output gripping force is plotted in Fig. 6, with respect to different gripping positions for the 0.6-mm diameter needle under the 10-N actuation. When the gripping position has a distance of 2.6 mm from the joint pin, the output gripping force can reach 62.67 N. When the distance from the joint pin is greater than 2.6 mm, the output force decreases with the increased distance.

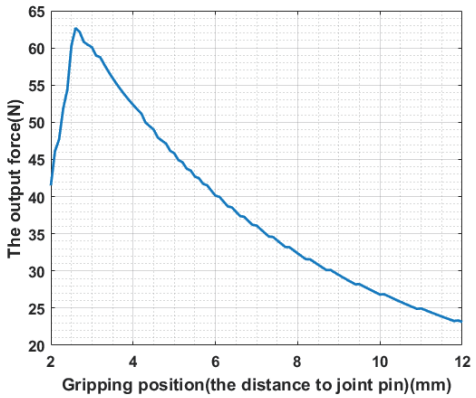

Figure 6. The gripping force with respect to the griping position under the actuation force of 10 N

E. Comparison

The proposed sliding-pin needle driver is compared with the manual laparoscopic needle driver in Fig. 1(a) and the 8-mm da Vinci EndoWrist *large needle driver* for their output gripping forces, when the actuation forces are all 10 N and the needle is gripped 8 mm from the joint pin. The comparison is plotted in Fig. 7.

The output gripping force of the manual laparoscopic needle driver is simulated according to the measured structural dimensions. And it is always less than the output force of the 8-mm da Vinci EndoWrist *large needle driver*, where the jaws are actuated by a pair of pulleys (this leading to a constant output gripping foce). When the jaw opening angle is less than 21.7°, the output force of the sliding-pin needle driver is greater than that of the 8-mm da Vinci EndoWrist *large needle driver*.

The output force of the da Vinci *large needle driver* can reach 21.64 N at the tip when the opening angle is close to 0° as reported by [8]. This means an actuation force, much larger than 10 N, has been used. When the opening angle is larger, the output force decreases [9].

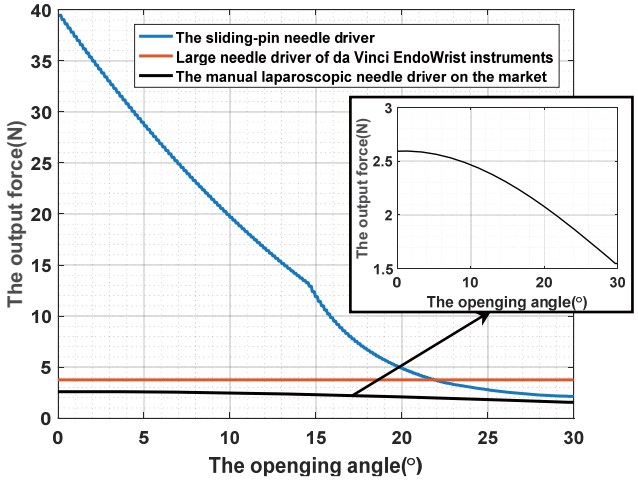

Figure 7. Comparison of the output forces among the three needle drivers

IV. Design Characterization

Simulation and experimental characterizations of the proposed sliding-pin needle driver were carried out to validate the design.

A. Finite Element Analysis

The finite element analysis was first conducted for the sliding-pin needle driver. The 3D model of the opening jaw is imported into ANSYS for the analysis.

In order to obtain a conservative estimation of the jaw's load-bearing capacity, worst-case scenario loading conditions are constructed by simulating the opening jaw with the contact at the first tooth and an opening angle of $\theta = 0°$.

When the input actuation force is applied to the sliding pin, the contact forces between the pin and the Slot-1 in the opening jaw can be calculated, neglecting the friction. The output gripping force can also be obtained. These forces exerted on the opening jaw are designated in the ANSYS model and the stress distributions under the 10-N and 50-N actuation input forces can be obtained as in Fig. 8.

Due to the strength, biocompatibility and machinability, medical grade stainless steel is selected to fabricate the needle driver. The maximum equivalent stress, 100.42 MPa, occurs at a point in the Slot-1 curve when the actuation is 50 N. The stresses in the jaw remain relatively low compared to the yield strength of the selected stainless steel material.

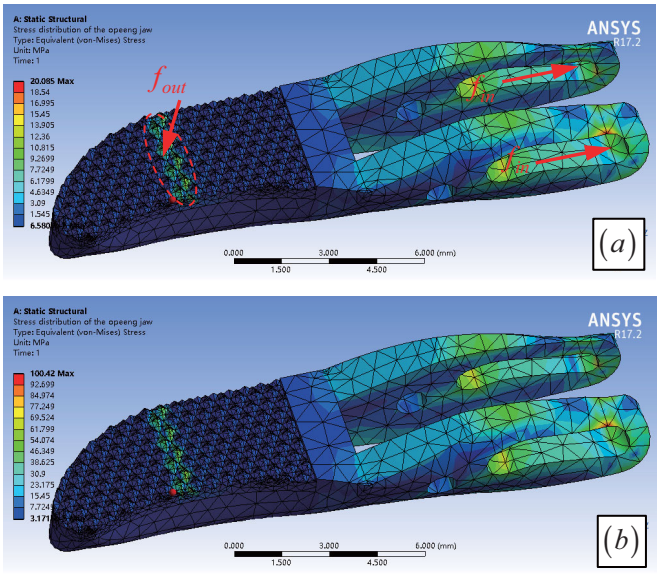

Figure 8. Stress distribution of the opening jaw with the actuation forces of: (a) 10 N, and (b) 50 N

B. Experimental Validations

The proposed needle driver was fabricated as shown in Fig. 9(a). Experimental validations were conducted to evaluate the needle driver prototype.

The needle driver should hold the suture needle steadily by generating enough gripping forces. However, it is relatively challenging to accurately measure the gripping forces. Instead, the pull-off force, with which the needles were pulled off the closed jaws of the needle driver, was measured.

The needle used in this experiment was a circular one with a diameter of 0.6 mm at one end (the other end has a sharp point).

The experiment setup that was used to measure the pull-off force is shown in Fig. 8(b). This experiment setup includes a lead screw guide that can be locked, two digital force gauges, an adjustable vice, and an adapter plate that is shown in Fig. 10.

The lead screw guide and the adjustable vice are both fixed to the workbench. One of the digital force gauges was attached to the nut block of the lead screw guide, as well as connected with the nitinol rod for the needle driver actuation. The adjustable vice clamps the needle driver. While rotating the lead screw, the actuation force will be exerted and measured by the digital force gauge.

The other force gauge was used to measure the pull-off force, as shown in Fig. 10, where an adapter plate was used to load the gripped needle. The needle was gripped at approximately 8 mm from the joint pin.

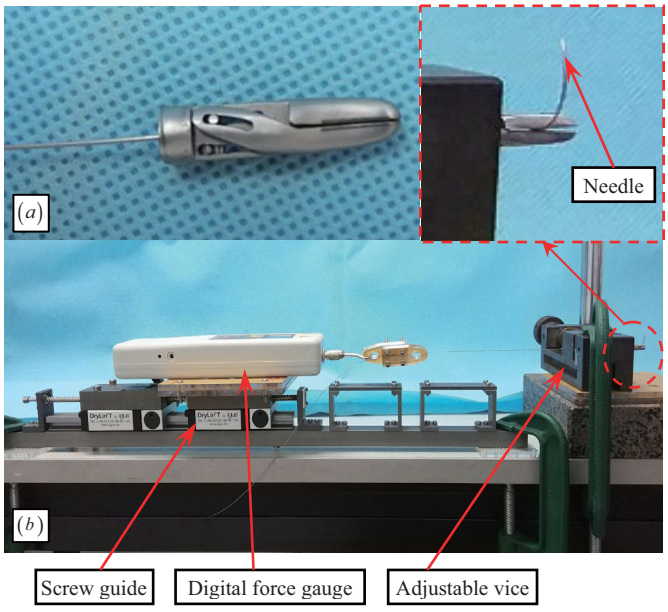

Figure 9. Experimental validation: (a) the prototype of the sliding-pin needle driver, and (b) the experiment setup

When the actuation input force is 10 N, the measured average pull-off force of the needle driver was 20.11 N, from five trials. The test results are listed in Table II when the input actuation forces were increased from 10 N to 50 N.

The experimental results on the pull-off forces indicate the gripping capabilities of the needle driver.

When the actuation input force is 10 N, a 40-N gripping force should be able to generate a pull-off force approximately 12 N to 16 N, using a friction coefficient from 0.3 to 0.4. The actual pull-off force was larger, due to fact that the needle is a circular one and its geometrical shape helped increase the pull-off force.

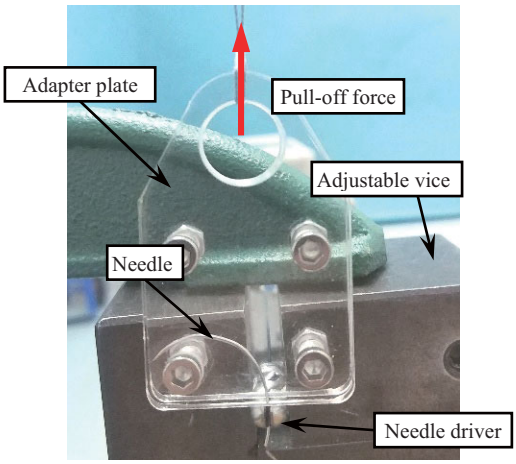

Figure 10. Pull-off force tests

TABLE I. AVERAGE PULL-OFF FORCES OF THE NEEDLE DRIVER

Needle Driver	Input Actuation Forces				
	10 N	20 N	30 N	40 N	50 N
Pull-off Force (N)	20.11	24.14	40.86	55.33	67.33

V. CONCLUSIONS AND FUTURE WORKS

This paper presents the design, construction and validation of a sliding-pin needle driver for a continuum surgical robot. The design aims at generate enough gripping forces under a limited actuation input. A curved slot was designed at the opening jaw for amplifying the actuation effect of the input force.

The model-based design approach is elaborated. A comparison of the output gripping forces among the sliding-pin needle driver, the *large needle driver* of the da Vinci EndoWrist tool and a manual laparoscopic needle driver was reported to indicate the superior gripping capability of this needle driver, under a very limited input actuation force.

Finite element analysis was carried out to verify the strength of the needle driver. Experimental validations were performed to show the gripper can hold a suture needle firmly.

Future works would mainly be the integration of the needle driver into a continuum surgical robot, in order to eventually fully verify the effectiveness of the proposed idea.

REFERENCES

[1] A. Cuschieri, "Laparoscopic Surgery in Europe: Where Are We Going," *Cirugia Espanola,* vol. 79, No.1, pp. 10-21, Jan 2006.

[2] R. H. Taylor and D. Stoianovici, "Medical Robotics in Computer-Integrated Surgery," *IEEE Transactions on Robotics and Automation,* vol. 19, No.3, pp. 765-781, 2003.

[3] C. Bergeles and G.-Z. Yang, "From Passive Tool Holders to Microsurgeons: Safer, Smaller, Smarter Surgical Robots," *IEEE Transactions on Biomedical Engineering,* vol. 61, No.5, pp. 1565-1576, May 2014.

[4] M. C. Cavusoglu, M. Cohn, F. Tendick, and S. Sastry, "A Laparoscopic Telesurgical Workstation," *IEEE Transactions on Robotics and Automation,* vol. 15, No.4, pp. 728-739, 1999.

[5] G. S. Guthart and J. K. Salisbury, "The Intuitive™ Telesurgery System: Overview and Application," in *IEEE International Conference on Robotics and Automation (ICRA)*, San Francisco, CA, 2000, pp. 618-621.

[6] P. Berkelman and J. Ma, "A Compact Modular Teleoperated Robotic System for Laparoscopic Surgery," *The International Journal of Robotics Research,* vol. 28, No.9, pp. 1198-1215, 2009.

[7] B. Hannaford, J. Rosen, D. W. Friedman, H. King, P. Roan, L. Cheng, D. Glozman, J. Ma, S. N. Kosari, and L. White, "Raven-II: An Open Platform for Surgical Robotics Research," *IEEE Transactions on Biomedical Engineering,* vol. 60, No.4, pp. 954-959, April 2013.

[8] P. Mucksavage, D. C. Kerbl, D. L. Pick, J. Y. Lee, E. M. McDougall, and M. K. Louie, "Differences in Grip Forces Among Various Robotic Instruments and da Vinci Surgical Platforms," *Journal of Endourology,* vol. 25, No.3, pp. 523-528, March 2011.

[9] C. Lee, Y. H. Park, C. Yoon, S. Noh, C. Lee, Y. Kim, H. C. Kim, H. H. Kim, and S. Kim, "A Grip Force Model for the Da Vinci End-Effector to Predict a Compensation Force," *Medical & Biological Engineering & Computing,* vol. 53, No.3, pp. 253-261, March 2015.

[10] D. Trivedi, C. D. Rahn, W. M. Kier, and I. D. Walker, "Soft Robotics: Biological Inspiration, State of the Art, and Future Research," *Applied Bionics and Biomechanics,* vol. 5, No.3, pp. 99-117, Sept 2008.

[11] N. Simaan, K. Xu, A. Kapoor, W. Wei, P. Kazanzides, P. Flint, and R. H. Taylor, "Design and Integration of a Telerobotic System for Minimally Invasive Surgery of the Throat " *International Journal of Robotics Research,* vol. 28, No.9, pp. 1134-1153, 2009.

[12] J. Ding, R. E. Goldman, K. Xu, P. K. Allen, D. L. Fowler, and N. Simaan, "Design and Coordination Kinematics of an Insertable Robotic Effectors Platform for Single-Port Access Surgery," *IEEE/ASME Transactions on Mechatronics,* vol. 18, No.5, pp. 1612-1624, Oct 2013.

[13] K. Xu, J. Zhao, and M. Fu, "Development of the SJTU Unfoldable Robotic System (SURS) for Single Port Laparoscopy," *IEEE/ASME Transactions on Mechatronics,* vol. 20, No.5, pp. 2133-2145, Oct 2015.

[14] J. Burgner-Kahrs, D. C. Rucker, and H. Choset, "Continuum Robots for Medical Applications: A Survey," *IEEE Transactions on Robotics,* vol. 31, No.6, pp. 1261-1280, Dec 2015.

[15] D. Sallé, F. Cepolina, and P. Bidaud, "Surgery Grippers for Minimally Invasive Heart Surgery," in *IEEE International Conference on Intelligent Manipulation and Grasping (IMG)*, Genova, Italy, 2004.